Journal of Solid State Chemistry 181 (2008) 2364–2369

Contents lists available at ScienceDirect

Journal of Solid State Chemistry

journal homepage: www.elsevier.com/locate/jssc

Temperature dependence of the cation distribution in $ZnFe_2O_4$ measured with high temperature neutron diffraction

F. Bræstrup [a,*], B.C. Hauback [b], K.K. Hansen [a]

[a] Fuel Cells and Solid State Chemistry Department, National Laboratory for Sustainable Energy, Frederiksborgvej 399, 4000 Roskilde, Denmark
[b] Physics Department, Institute for Energy Technology, NO-2027 Kjeller, Norway

ARTICLE INFO

Article history:
Received 22 January 2008
Received in revised form
6 May 2008
Accepted 11 May 2008
Available online 24 May 2008

Keywords:
Spinel-type oxide
Conductivity
Powder diffraction

ABSTRACT

$ZnFe_2O_4$ has a spinel-type structure with Zn^{2+} ions located mainly on tetrahedral sites and Fe^{3+} ions located on octahedral sites. $ZnFe_2O_4$ was synthesized in air by a solid state reaction and characterized with X-ray diffraction, high temperature neutron diffraction, resistivity measurements and dilatometry. The distribution of cations in $ZnFe_2O_4$ was measured from 298 to 1243 K and results show that above 673 K the cations start to redistributed in the structure. $ZnFe_2O_4$ has a semi-conducting behavior at room temperature, but at temperatures above 905 K the conductivity decreases as the result of an Fe–Fe interaction between octahedral sites.

1. Introduction

Spinels are a very large class of compounds which are isotypic with the mineral spinel $MgAl_2O_4$. Spinel materials are widely used in the industry because of their usefulness as magnetic materials, semi-conductors, pigments, catalysts and refractories. Most of them are oxides but also sulphates, selenides and tellurides are know to have the spinel structure [1–3]. The spinel structure of oxides (AB_2O_4) is build up around O^{2-} ions which form a face-centered close cubic packing (CCP) sequence, with 16 tetrahedral sites and 64 octahedral sites per unit cell. The CCP layers of oxygen are stacked parallel to {111}, resulting in alternating layers of octahedral sites and tetrahedral sites. Several different cations can be introduced in the structure which leads to a variety of different charge combinations e.g. $SnMg_2O_4$, $LiCrTiO_4$ or Na_2WO_4 [4–6]. Spinels are traditionally divided into two different ideal types of structures: the *normal* spinel structure and the *inverse* spinel structure. In normal spinels, A ions are located on tetrahedral sites and B ions on octahedral sites. Inverse spinels have half the B ions located on tetrahedral sites, while the rest of the B ions and the A ions occupies the octahedral sites. The cation distribution is often quantified with the parameter γ, which corresponds to the fraction of A ions on the octahedral sites. Spinel-type materials with a normal spinel structure will have $\gamma = 0$, whereas inverse spinel structures will have a γ-value of 1.

$ZnFe_2O_4$ has an almost normal spinel structure with Zn^{2+} located on tetrahedral sites and Fe^{3+} located on octahedral sites. $ZnFe_2O_4$ is a promising electrode material in NO and NO_2 sensors [7,8] and the material has also received much interest as a possible sensor material for organic compounds such as ethanol, acetone and propanol [9,10]. Other reports also indicate that $ZnFe_2O_4$ is active toward Cl_2 gas-sensing [11].

O'Neill [12] have studied the temperature dependence of the cation distribution with X-ray diffraction by quenching the samples in water but he was not able to refine the occupancies on the tetrahedral sites. Kamiyama et al. [13] and Ligenza [14] analyzed the cation distribution by neutron diffraction but only in the temperature range of 4.2−300 K. To our knowledge no in situ high temperature neutron diffraction (HTND) have been preformed on $ZnFe_2O_4$. HTND was therefore used in this study for precise determination of the distribution of the cations at different temperatures in $ZnFe_2O_4$.

2. Experimental details

2.1. Sample preparation and X-ray diffraction

$ZnFe_2O_4$ was synthesized with a solid state reaction using powder of metal oxides (ZnO 99.99% (Alfa Aesar) and α-Fe_2O_3 99.9% (Alfa Aesar)). The powder was mixed in an agate mortar and calcined at 1173 K for 30 h with a ramp rate of 373 K/h. The powder was then crushed in an agate mortar and the calcination process was repeated. The spinel powder was analyzed in air at

* Corresponding author. Fax: +45 46775858.
E-mail address: frantz.braestrup@risoe.dk (F. Bræstrup).

0022-4596/$ - see front matter © 2008 Elsevier Inc. All rights reserved.
doi:10.1016/j.jssc.2008.05.028

room temperature with X-ray diffraction on a theta–theta STOE diffractometer with a Cu anode. The powder was measured in the 2θ-range from 10° to 130° with a step width of 0.02° and an exposure time of 10 s. The powder was pressed on a CompaC PRESS at 1 ton for 30 s into an elongated rod ($4 \times 4 \times 35$ mm) which were placed in a rubber sleeve and pressed isostatically at 50 ton for 20 s using a STENHØJ 100 PRESS. The samples were then calcined at 1473 K for 6 h with a ramp rate of 373 K/h. The elongated rod was cut into two pieces: one was used for resistivity measurements ($4 \times 4 \times 18$ mm) while the other one ($4 \times 4 \times 12$ mm) was used to determine the linear thermal expansion coefficient, α.

2.2. Dilatometry

The linear thermal expansion was measured by dilatometry in air (50 ml/min) using a NETZSCH DIL 402C dilatometer with a sample load of 30 000 cN. The sample-rod was heated from room temperature up to 1273 K and back at 2 K/min. The sample remained at 1273 K for 2 h. Data were calibrated to an Al_2O_3 standard at identical conditions.

2.3. Four-point DC resistivity measurement

Platinum paste was applied to each end of the elongated rod and contacted with platinum leads. Two platinum potential probes with a fixed distance were positioned on one side of the bar. The data collection was made with an in-house data acquisition software, ELCHEMEA. The resistivity was measured every 5 min from room temperature to 1323 K and back again with a 2-h dwell at every 50 K interval and using a ramp rate of 2 K/min. In order to correct the resistivity for the porosity of the sample, the density of the elongated rod was measured by the Archimedes principle.

2.4. HTND

HTND was measured with a high-resolution powder neutron diffractometer, installed at a 2 MW JEEP II reactor at the Institute for Energy Technology in Kjeller, Norway. The powder was placed in a quartz tube inside a furnace and measured in air with a 2θ-range of 10–130°, a step width of 0.05° and a wavelength of 1.555 A using a Ge(511) monochromator. Two detector banks, each covering 20° in 2θ and containing seven ^{3}He position sensitive detectors stacked on top of each other, were used to record the neutron diffraction pattern. A more detailed description of the diffractometer can be found elsewhere [15].

Rietveld refinements were carried out using the program Jana2000 [16]. The neutron scattering lengths and the X-ray form factors were taken from the Jana2000 library. Pseudo-Voigt profile functions were used, and the background was modeled with a 10 terms Legendre polynomials.

3. Results

3.1. X-ray diffraction

X-ray powder diffraction showed that the material was a single spinel phase. The Rietveld refinement gave no satisfying result of the site occupancies because of the relatively small difference in the electron density of the cations. Therefore was only a Le Bail fit made in order to determine the unit cell parameter, $\mathbf{a} = 8.4309(2)$ A, at room temperature.

3.2. HTND

Fig. 1 shows the neutron diffraction patters of the spinel measured from 298 to 1243 K. Total 21–22 peaks were used in the refinement depending on the temperature. The neutron diffraction patterns were refined with Rietveld methods using JANA2000. All diffraction patterns were refined with the space group $Fd\bar{3}m$ (no. 227, origin choice 1) [17], but diffraction patterns measured at temperatures above 873 K were also refined with the space group $I4_1/amd$ (no. 141), which is reported for different spinel-type materials [18]. This was done in order to see if changes at the octahedral sites resulted in at change of symmetry, but refinements gave no satisfying results. Site occupancies of Zn and Fe were coupled not only between elements on the same lattice site, but also between the tetrahedral and the octahedral site. Cations on same lattice sites where assigned the same isotropic displacement parameter, U_{iso}. No impurity phases were detected as also found by X-ray diffraction. Table 1 shows an example of the refined structural parameters for $ZnFe_2O_4$ at 873 K and Fig. 2 shows the corresponding fitted neutron diffraction pattern. Refined parameters at different temperatures are shown in Table 2.

Fig. 3a shows the increase of the unit cell as a function of temperature. From 298 to 873 K, **a** increases linearly with a rate $7.3(4) \times 10^{-5}$ A K^{-1}. At 873 K the rate increases to $1.01(3) \times 10^{-4}$ A K^{-1} which is 38% faster than in the low temperature range.

Refinements show that the tetrahedrons are undistorted (not shown in Table 3) within experimental errors and change of bond distances does not seem to follow a trend through the measured temperature range. The octahedrons are on the other hand slightly distorted with increasing bond distances as a function of temperature. However, the bond distances on the octahedral sites

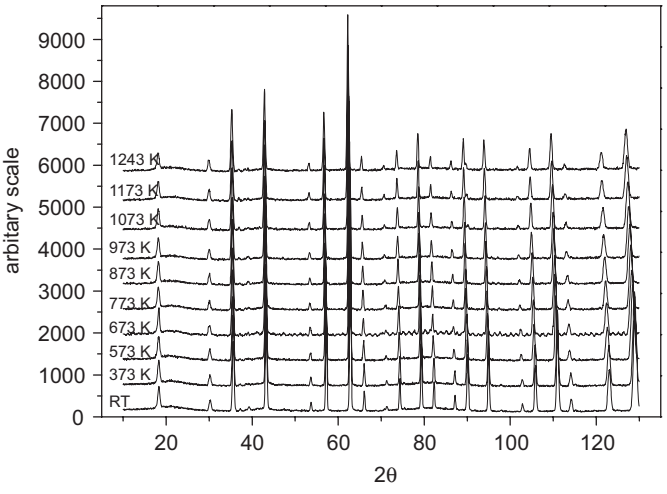

Fig. 1. HTND profiles of $ZnFe_2O_4$ at measured temperatures.

Table 1
Refined structural parameters of $ZnFe_2O_4$ at 873 K

Atom	Site	Occupancy	x	y	z	U_{iso}
Zn1	8a	0.0357(2)	0	0	0	0.0354(6)
Fe1	8a	0.0059(2)	0	0	0	0.0354(6)
Zn2	16d	0.0119(4)	0.625	0.625	0.625	0.0204(4)
Fe2	16d	0.0715(2)	0.625	0.625	0.625	0.0204(4)
O	32e	0.16667	0.3851(2)	0.3851(2)	0.3851(2)	0.0300(6)

Occupancies are given by the multiplicity of the site symmetry divided by the multiplicity of general sites.

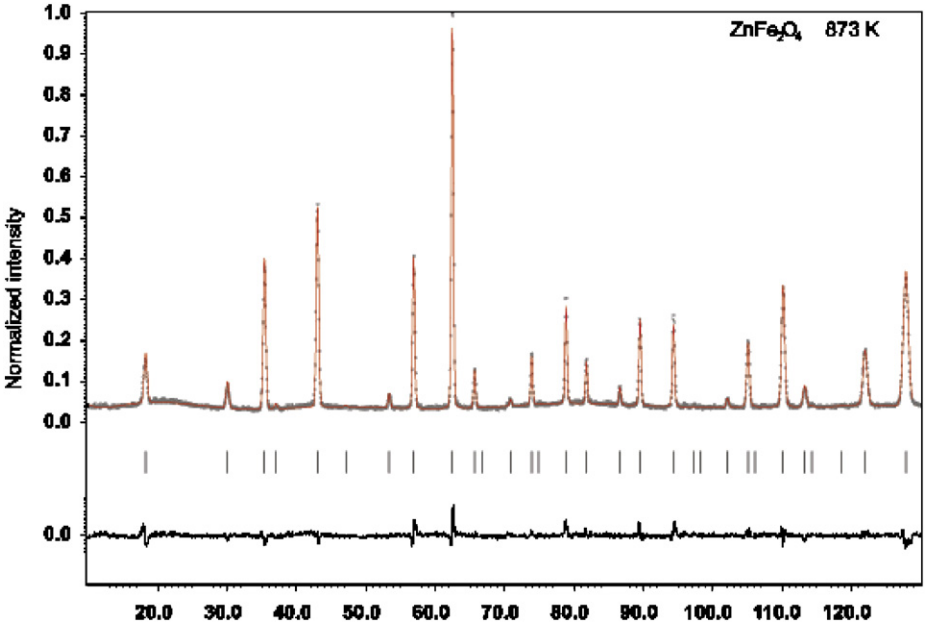

Fig. 2. Observed (gray) and calculated (red) intensities from Rietveld refinements of $ZnFe_2O_4$ at 873 K. The difference curve and the position of the Bragg reflections are shown in the lower part of the diffractogram.

Table 2

R-values, 'goodness of fit', gof, unit cell parameters, **a**, the position of oxygen, O_x, and isotropic displacement parameters, U_{iso} ($Å^2$), from the Rietveld refinements of the HTND patterns

Temp. (K)	R_p	wR_p	gof	**a** (Å)	O_x	U_{iso}, [4]	U_{iso}, [6]	U_{iso}, O_x
298	6.02	7.63	1.50	8.4371(4)	0.3849(1)	0.0164(7)	0.0124(4)	0.0175(5)
373	6.88	9.08	1.94	8.4473(6)	0.3844(2)	0.0163(7)	0.0139(8)	0.0196(9)
573	7.00	9.17	1.88	8.4573(6)	0.3852(1)	0.025(3)	0.0185(6)	0.0234(8)
673	7.05	9.18	1.96	8.4655(6)	0.3842(2)	0.026(1)	0.0231(6)	0.0303(9)
773	6.96	9.11	1.47	8.4753(3)	0.3853(2)	0.029(2)	0.0214(5)	0.0291(7)
873	6.01	7.66	1.25	8.4819(4)	0.3852(1)	0.0354(9)	0.0204(4)	0.0300(7)
973	5.89	7.38	1.20	8.4906(4)	0.3849(1)	0.0370(9)	0.0225(4)	0.0322(7)
1073	6.25	7.97	1.31	8.5025(4)	0.3846(2)	0.0394(9)	0.0251(5)	0.0345(7)
1173	6.02	7.70	1.25	8.5120(4)	0.3845(2)	0.0401(9)	0.0267(5)	0.0378(8)
1243	5.98	7.70	1.40	8.5186(4)	0.3840(2)	0.0414(9)	0.0272(5)	0.0415(8)
*373	6.52	8.27	1.34	8.4473(4)	0.3849(1)	0.0197(7)	0.0138(4)	0.0198(6)
*573	6.46	8.20	1.34	8.4573(4)	0.3850(2)	0.028(8)	0.0170(4)	0.0265(6)

Values in square brackets refer to the coordination number of the cations. Temperatures marked with, *, refer to the diffraction patterns measured during cool down. No correlation coefficients where lager than $\rho_{ij} = 0.72$. Estimated standard deviations in parentheses.

do not follow a linear trend in the whole temperature range. A sudden increase is observed at 873 K as can be seen in Fig. 3b. The bond length at 373 and 673 K is slightly higher than would be expected. Same phenomenon can also be detected in the increasement of the volume (Fig. 3c).

Figs. 4a and b show the occupancy of Zn and Fe on the tetrahedral and the octahedral sites as a function of temperature. In the temperature range of 298–673 K the site occupancies are unchanged with 91% ($\gamma = 0.09$) of the Zn at the tetrahedral lattice site. At 773 K there is a sudden change in occupancies towards a higher cation ordering ($\gamma = 0.03$), but from 773 to 1243 K the site occupancies changes almost linearly and at 1243 K only 77% ($\gamma = 0.23$) of the Zn are still located at the tetrahedral site. After cooling down the sample a new diffraction pattern was recorded at 573 and 373 K. Results show that the site occupancies are almost identical to those found while heating up the sample. The sudden change in occupancies at 773 K was tried refined by constraining the occupancies, so they followed the main trend of the graph; however, it was not possible to obtain reasible isotropic displacement parameters of any of the atoms and *R*-values and goodness of fit did not improve significantly. A few correlation coefficients also increased, $\rho_{ij} > 0.8$.

3.3. Resistivity measurement

Fig. 5a shows the four-point DC specific resistivity of $ZnFe_2O_4$ as well as the temperature profile. Data have been corrected for the open porosity (1.7%). $ZnFe_2O_4$ was a semi-conductor already at room temperature, but after heating the sample, the semi-conducting behavior disappeared at around 390 K.

Fig. 5b shows an Arrhenius plot of the specific conductivity as a function of temperature. The graph shows a semi-conducting behavior with a linear increase in conductivity but with a distinct change of slope at 905 K. The data were fitted with [19]:

$$\sigma = \sigma_0 T^{-1} \exp \frac{-E_a}{k_B T} \quad (1)$$

where σ is the specific conductivity and k_B and T are the Boltzmann constant and the temperature, respectively. The

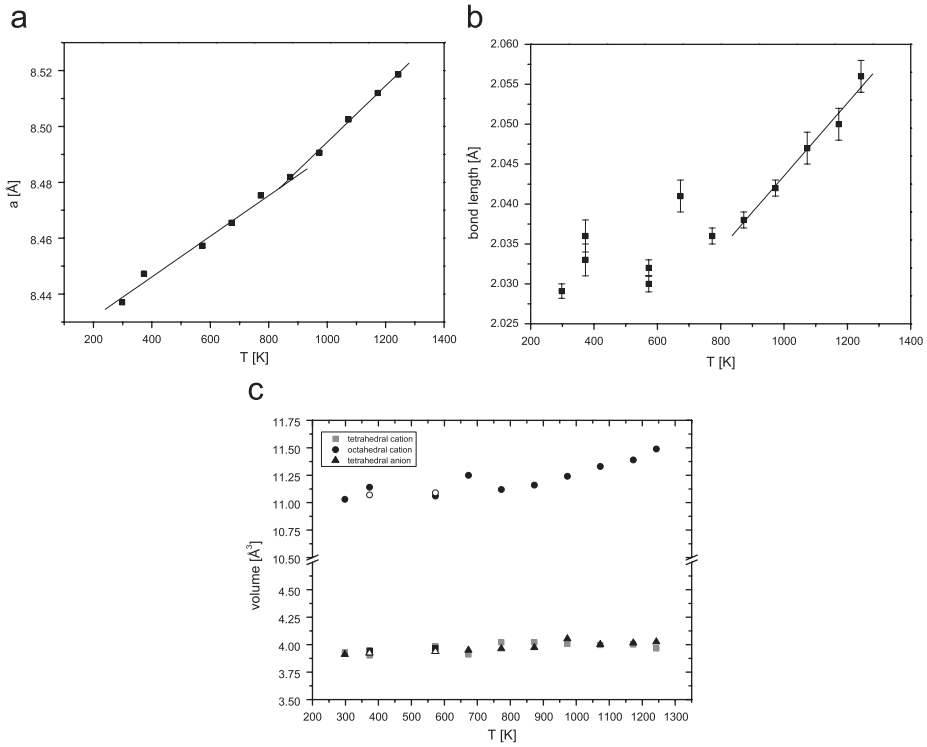

Fig. 3. (a) Unit cell parameters and (b) bond length of the octahedron as function of temperature measured with HTND. Two clear linear trends can be detected in the case of the unit cell parameter. (c) shows the volume of the polyhedrals as function of temperature. △ and ○ represent the measurements made during the cooling stage. Error bars on the unit cell parameter and the volumes are shown by the radius of the points.

Table 3
Bond lengths and bond angles from the Rietveld refinement of the HTND patterns

Temp. (K)	[4] (Å)	[6] (Å)	∠[6]$_1$ (deg)	∠[6]$_2$ (deg)	∠[6] [4] (deg)
298	1.972(1)	2.027(3)	94.82(4)	85.18(4)	121.92(4)
373	1.966(2)	2.036(2)	94.54(6)	85.46(6)	121.11(7)
573	1.982(1)	2.032(1)	94.99(4)	85.01(4)	121.80(6)
673	1.968(2)	2.041(2)	94.48(7)	85.52(7)	122.16(9)
773	1.986(2)	2.036(1)	95.00(4)	85.00(4)	121.80(7)
873	1.986(1)	2.038(1)	94.95(5)	85.05(5)	121.84(6)
973	1.984(2)	2.042(2)	94.81(3)	85.19(3)	121.93(4)
1073	1.982(2)	2.047(2)	94.66(7)	85.34(7)	122.03(8)
1173	1.983(2)	2.050(2)	94.61(7)	85.39(7)	122.07(8)
1243	1.977(2)	2.056(2)	94.35(7)	85.65(7)	122.24(8)
*373	1.972(1)	2.030(1)	94.82(4)	85.18(4)	121.92(5)
*573	1.978(2)	2.033(3)	94.87(6)	85.13(6)	121.81(6)

The [4] and [6] represent the cation–oxygen bond length of cations located on tetrahedral or octahedral coordinated lattice sites. The ∠[4] and ∠[6] represent the oxygen–cation–oxygen bond angles, whereas ∠[4] [6] represent the cation–oxygen–cation bond angles between two different coordinated cations. Bond angles show that the octahedrons are slightly disturbed, whereas the tetrahedrons are undisturbed within experimental errors. Temperatures marked with, *, refer to the diffraction patterns measured during cool down. Estimated standard deviations in parentheses.

activation energies in the lower and upper temperature range were calculated to $E_a = 0.248(1)$ and $0.126(4)$ eV, respectively.

3.4. Dilatometry

Fig. 6 shows the relative linear expansion of $ZnFe_2O_4$ as function of temperature. The curve is slightly bended toward a larger relative expansion coefficient, α, at high temperatures (~823 K) and with only a small hysteresis shown below 600 K. α, defined as $\alpha = 1/L \times \delta L/\delta T$, changes from $\alpha = 5.7 \times 10^{-7}\,K^{-1}$ at 700 K to $6.3 \times 10^{-7}\,K^{-1}$ at 900 K.

4. Discussions

The increase in unit cell parameters (Fig. 3a) consists of two linear trends. The first trend from room temperature to ~873 K is related to a simple thermal expansion due to the increase of lattice vibrations. However, the sudden increase of the unit cell parameter at ~873 K seems to be related to the increasing disorder of the cations. When the Zn ions jump from a tetrahedral lattice sites to a octahedral site, the volume of the octahedron will increase due to larger effective ion radius of Zn^{2+} ([4]: 0.60 Å, [6]: 0.74 Å) compared to Fe^{3+} ([4]: 0.63 Å, [6]: 0.65 Å) [20]. This also explains why the increase of the bond length at the octahedral site coincides with the increase of the unit cell parameter. The tetrahedral site does not seem to follow the same trend as the octahedrons, which can also be explained by the similarity of the ion radii of Zn^{2+} and Fe^{3+}. The octahedrons become less distorted at high temperatures, since the thermal energy makes the lattice expand. Refinements also indicated a decrease in atomic displacements of the oxygen position, but the uncertainties are too high to give a clear image.

It cannot be ruled out completely that a small amount of ZnO evaporates at high temperatures, leaving some of the Fe^{3+} to be chemically reduced to Fe^{2+}. The effective ion radius of Fe^{3+} and Fe^{2+} in a tetrahedral coordination are practically the same (0.63 Å), whereas the effective ion radius of Fe^{3+} (0.65 Å) and Fe^{2+} (0.78 Å) on an octahedral site differs by 20%. If any Fe^{2+} ions are found in the structure, they will mainly be located at octahedral sites [21], and therefore they will certainly contribute to the expansion of the octahedrons. Measurements of the relative linear thermal expansion also show a slightly positive deviation at 823 K, but it seems to related to the cation disorder and not the oxidation state of iron. Similar observations was observed by Brabers [22] on stoichiometrically synthesized $ZnFe_2O_4$. However, he also observed that a small surplus of Fe^{2+} incorporated into the

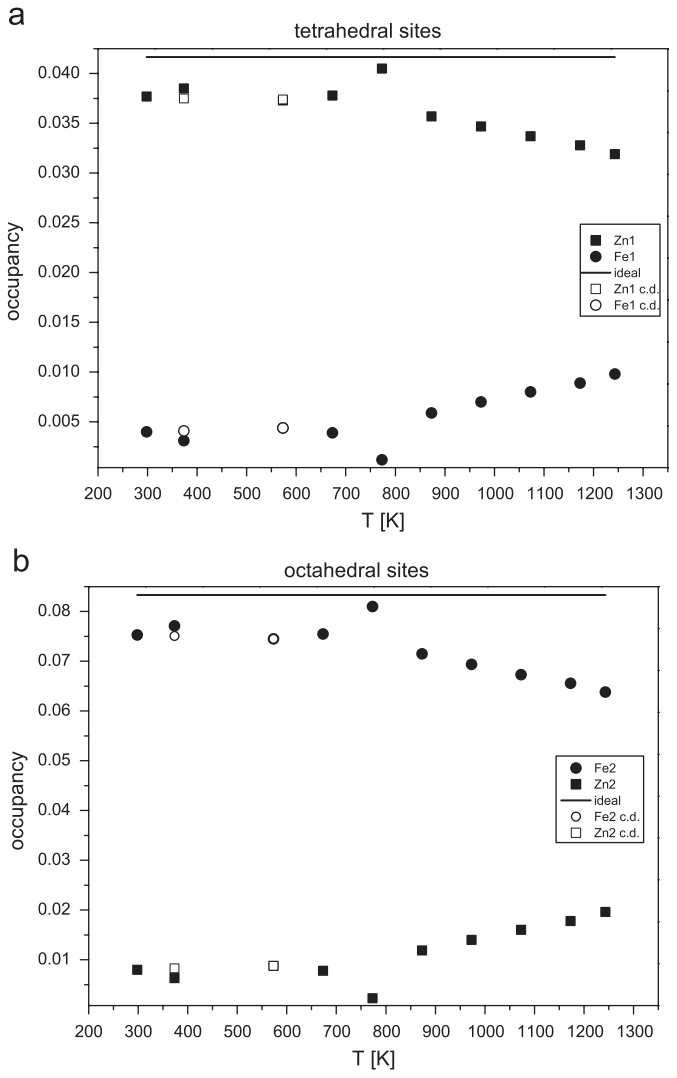

Fig. 4. Occupancies on (a) the tetrahedral and (b) the octahedral site in $ZnFe_2O_4$ as a function of temperature. ■ and ● represent Zn and Fe, respectively. □ and ○ represent the measurements made during the cooling stage. The upper horizontal line shows the ideal occupancy. Error bars are shown by the radius of the points.

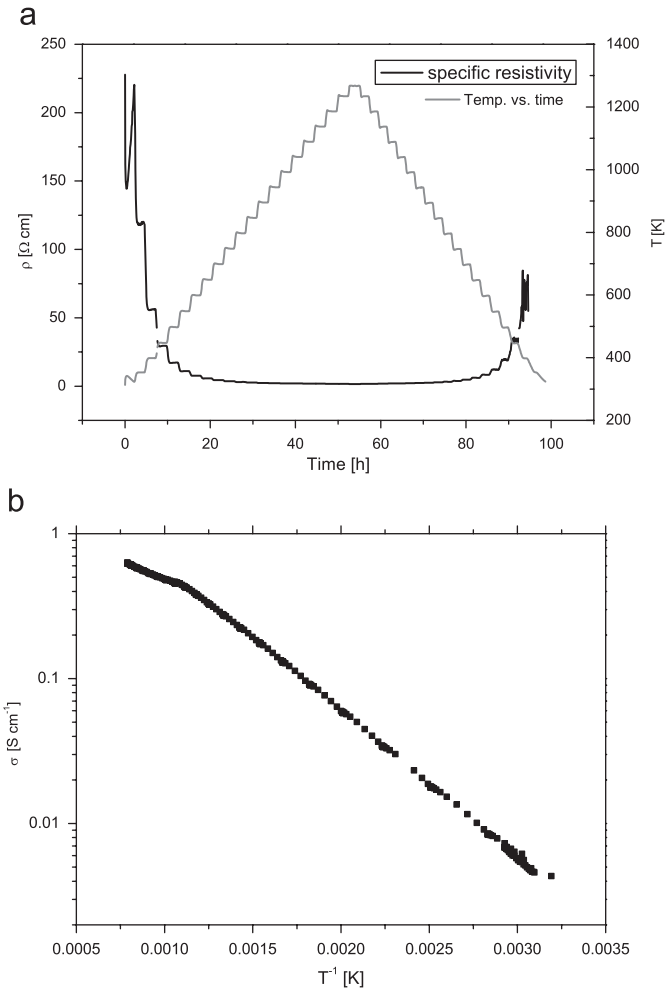

Fig. 5. (a) The specific resistivity as a function of time and temperature. (b) The specific conductivity as a function of temperature shows that $ZnFe_2O_4$ is a relatively good semi-conductor already at room temperature. At temperature above 905 K the conductivity decreases slightly.

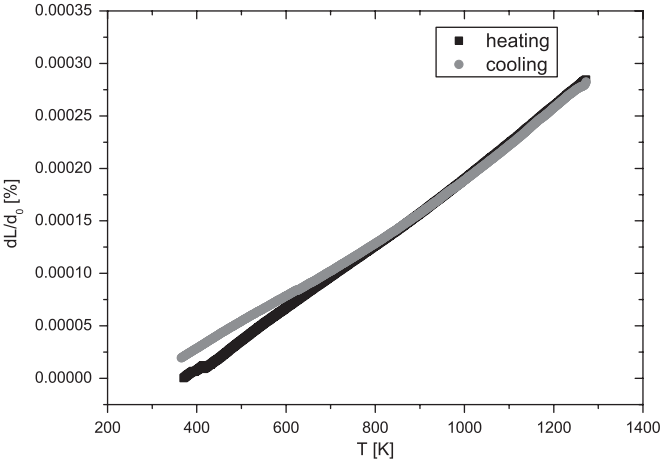

Fig. 6. The relative linear thermal expansion measured in air from room temperature to 1273 K.

structure will make the relative thermal expansion decrease at ~873 K. Therefore it is assumed that the concentration of Fe^{2+} in our sample is small since the starting material was mixed stoichiometrically and calcined at 1173 K where no substantial ZnO evaporation exists and because we do not see a negative deviation from the main trend of the relative thermal expansion.

Refinements of the occupancies show that the cations start to jump between lattice sites at 773 K. The sudden increase of ordering observed at 773 K reflects both the kinetics and the thermodynamics of the system [23]. At low temperatures the sample is not in equilibrium and the kinetic controls the cation order–disorder. At high temperatures the spinel is in equilibrium with respect to the cation order–disorder, reflecting the thermodynamic drive towards high temperature disorder. The increase in order at 773 K results from the starting value being lower than equilibrium and as soon as the temperature is high enough, the occupancies begin to converge towards the order–disorder equilibrium. The cations start to jump between lattice sites at a lower temperature compare to the sudden increase in octahedrals. This shows that the crystal structure (and with the help of the thermal lattice vibrations) can incorporate a certain amount of cation disorder without a distinct change of the unit cell volume.

The refinements of the HTND patterns also show that the cations switch back into there original lattice position when the sample is cooled down. However, the unsymmetrical behavior of the resistivity on Fig. 5a indicates that the occupancies are not

completely identical to the ones before heating the specimen. Otherwise the specific conductivity would be the same before and after heating the sample. The difference between the occupancies and the resistivity measurements is, however, most likely due to the fact that the samples used for the different measurements were exposed to different kind of temperature profile during 'cool down'.

Zn has closed atomic shells and will therefore not contribute directly to the conductivity. Only Fe can contribute to the conductivity. Anderson [24] pointed out that if the cation–anion–cation angle is 90° the domination interaction is a cation–cation interaction, whereas if the angle is 180° or as low as 120° the cation–anion–cation exchange interaction is assumed to be the dominant one. The cation–anion–cation angle between tetrahedral and octahedral sites is ~122° (Table 3), and therefore this interaction could have an influence on the conductivity, whereas the cation–anion–cation angle on tetrahedral sites (109.47°) is too low to cause a cation–anion–cation distinct interaction. It has been shown for $ZnFe_2O_4$ that Fe on a tetrahedral site and its 12 nearest Fe ions on octahedral sites form a cluster in which each of the Fe ion on the octahedral sites interact through an oxygen ion with an Fe ion on a tetrahedral site [13,25,26]. However, those experiments were preformed mainly at low temperatures. In the measured temperature range, the conductivity of $ZnFe_2O_4$ is mainly attributed to the Fe–O–Fe super exchange interactions between octahedral sites [21,27,28], where the transport property rises from hopping of localized d-electrons between cations on octahedral sites. In an ideal spinel structure cations on octahedral sties are distributed in such a way that we have a cation–anion–□–anion–cation, with □ representing an empty site. Structural defects are therefore the main key in creating the cation–anion–cation interaction in $ZnFe_2O_4$. At 905 K the conductivity decreases slightly and seems to be related to a direct cation–cation interaction between Fe atoms on octahedral sites (maximum bond length ~3 A). The activation energy, 0.126(4) eV, is very similar to the one found by Hosseinpour et al. [29] in $ZnFe_2O_4$ containing 0.5% Fe^{2+} on octahedral sites. This, however, does not support the observations of the thermal expansion as discussed earlier in this section. Similar high-temperature cation–cation interaction between octahedral sites has also been reported in Cu- and Ga-doped $ZnFe_2O_4$ [21,27,28], although it was attributed to the Cu–Cu interaction. However, these materials were only measured at a maximum temperature of 700 K which is far below our transition temperature.

5. Conclusion

$ZnFe_2O_4$ was synthesized as a solid state reaction and characterized with X-ray diffraction. HTND was preformed on a powder sample from 298 to 1243 K and refinements show that $ZnFe_2O_4$ has a almost normal spinel structure with $\gamma = 0.09$ below 673 K. Cations start to redistribute among tetrahedral and octahedral sites at temperatures above ~673 K, but they switch back to their original position when the sample is cooled down again. The expansion of the unit cell parameter and octahedrons increases rapidly at ~873 K which seems to be related to the larger Zn^{2+} ion substituting the smaller Fe^{3+} on the octahedral sites. Resistivity measurements reveal a semi-conducting behavior of $ZnFe_2O_4$ from room temperature to 905 K, which mainly arises from a Fe–O–Fe exchange interaction between octahedral sites. Above 905 K $ZnFe_2O_4$ shows a more metallic behavior which is attributed to the Fe–Fe interaction on octahedral sites.

Acknowledgment

We give our thanks to Dr. Bente Lebech for fruitful discussions concerning the structural analysis.

References

[1] O. Knop, K.I.G. Reid, R. Sutarno, Y. Nakagawa, Can. J. Chem. 46 (1968) 3463–3476.
[2] H. Duda, I. Jendrzejewska, T. Groń, S. Mazur, P. Zajdel, A. Kita, J. Phys. Chem. Solids 68 (2007) 80–86.
[3] T. Suzuyama, J. Awaka, H. Yamamotoa, S. Ebisu, M. Ito, T. Suzuki, T. Nakama, K. Yagasaki, S. Nagata, J. Solid State Chem. 179 (2006) 140–144.
[4] A.A. Al-Shahrani, J. Mater. Sci. 16 (2005) 193–196.
[5] M.A. Arillo, M.L. Lopez, M.T. Fernandez, M.L. Veiga, C. Pico, J. Solid State Chem. 125 (1996) 211–215.
[6] R.H. Busey, J.O.L. Keller, J. Chem. Phys. 41 (1964) 215–225.
[7] S. Zhuiykov, M. Muta, T. Ono, M. Hasei, N. Yamazoe, N. Miura, Electrochem. Solid-State Lett. 4 (2001) H19–H21.
[8] S. Zhuiykov, T. Ono, N. Yamazoe, N. Miura, Solid State Ionics 152–153 (2002) 801–807.
[9] G. Zhang, L. Chunsheng, C. Fangyi, J. Chen, Sensors & Actuators B 120 (2007) 403–410.
[10] K. Arshak, I. Gaidan, Mater. Sci. Eng. B 118 (2005) 44–49.
[11] J.Z. Zhang, D.H. Chen, L. Chen, Sensors Mater. 5 (2006) 227–282.
[12] H.S.C. O'Neill, Eur. J. Miner. 4 (1992) 571–580.
[13] T. Kamiyama, K. Haneda, T. Sato, S. Ikeda, H. Asano, Solid State Commun. 81 (1992) 563–566.
[14] S. Ligenza, Phys. Status Solidi B 75 (1976) 315–326.
[15] B.C. Hauback, H. Fjellvag, O. Steinsvoll, K. Johansson, O.T. Buste, J. Jorgensen, J. Neutron Res. 8 (2000) 215–232.
[16] V. Petříček, M. Dusek, L. Palatinus, Jana2000, The crystallographic computing system, Institute of Physics, Praha, Czech Republic, 2000.
[17] T. Hahn (Ed.), International Tables for Crystallography, third ed., vol. A, Wiley, New York, 1992.
[18] O. Crottaz, F. Kubel, H. Schmid, J. Mater. Chem. 7 (1997) 143–146.
[19] N.M. Tallan, Electrical Conductivity in Ceramics and Glass: Part A–B, Dekker, New York, 1974.
[20] C. Klein, C.S. Hurlbut, J.D. Dana, Manual of Mineralogy, vol. 21, Wiley, New York, 1998.
[21] M. Wen, Q. Li, Y. Li, J. Electron Spectrosc. Relat. Phenom. 153 (2006) 65–70.
[22] V.A.M. Brabers, J. Phys. IV France 7 (1997) C1233–C1236.
[23] S.A.T. Redfern, Eur. J. Miner. 14 (2002) 251–261.
[24] P.W. Anderson, Phys. Rev. 79 (1950) 350–356.
[25] F.K. Lotgering, J. Phys. Chem. Solids 27 (1966) 139–145.
[26] V. Šepelák, K. Tkáčová, V.V. Boldyrev, S. Wissmann, K.D. Becker, Physica B 234–236 (1997) 617–619.
[27] S.S. Ata-Allah, M.K. Fayek, M. Yehia, J. Magn. Magn. Mater. 279 (2004) 411–420.
[28] S.S. Ata-Allah, F.M. Sayedamed, M. Kaiser, A.M. Hashhash, J. Mater. Sci. 40 (2005) 2923–2930.
[29] A. Hosseinpour, H. Sadeghi, A. Morisako, J. Magn. Magn. Mater. 316 (2007) e283–e286.